

FINAL REPORT

Detection of Underwater Military Munitions by
a Synoptic Airborne Multi-Sensor System

SERDP Project MR-1630

JULY 2010

Michael J DeWeerts
BAE Systems Spectral Solutions, LLC

This document has been approved for public release.



This report was prepared under contract to the Department of Defense Strategic Environmental Research and Development Program (SERDP). The publication of this report does not indicate endorsement by the Department of Defense, nor should the contents be construed as reflecting the official policy or position of the Department of Defense. Reference herein to any specific commercial product, process, or service by trade name, trademark, manufacturer, or otherwise, does not necessarily constitute or imply its endorsement, recommendation, or favoring by the Department of Defense.

Table of Contents

1.0 Abstract..... 1

2.0 Objective..... 1

3.0 Background..... 1

 3.1 Existing Detection Methods..... 2

 3.2 Optical UXO Detection..... 2

 3.3 Optical-Acoustic UXO Detection..... 5

4.0 Materials and Methods..... 5

 4.1 Multispectral Imagery..... 7

 4.2 REVEAL..... 8

 4.2.1 Gate Profile Generation 9

 4.2.2 Ratio Image File Generation..... 9

 4.2.3 Distance Calibrated Relief Image Generation 10

 4.2.4 One Camera LIDAR 10

 4.2.5 Two camera LIDAR 11

 4.2.6 Dynamic Range and Glint..... 11

 4.3 Shearography 11

 4.3.1 System Configuration 11

 4.3.2 Shearography System Operation..... 14

 4.3.3 Data Processing and Analysis..... 15

 4.4 Field Experiment Set-Up 15

 4.4.1 Makai Pier..... 15

 4.4.2 Waikele Tunnel..... 17

5.0 Results..... 20

 5.1 Multi-Spectral Imagery..... 20

 5.2 REVEAL..... 22

 5.3 Shearography 22

6.0 Information Fusion and Automation..... 27

7.0 Conclusions and Future Direction 27

8.0 References..... 28

List of Tables

Table I. Synoptic Sensor Suite..... 6

Table II. Summary of Phenomenology Studies 6

List of Figures

Figure 1. Examples of UXO munitions, bio-fouled and encrusted with corals and algae..... 2

Figure 2. Wavelength-dependent attenuation of electromagnetic radiation in pure seawater..... 3

Figure 3. Attenuation rates versus wavelength for various water turbidity types 4

Figure 4. Remote-sensing reflectance spectra of different bottom types..... 4

Figure 5. Schematic overview of the mine-detection system for the SAMSS project. 6

Figure 6. Demonstration of glint and foam removal..... 7

Figure 7. REVEAL operation in laboratory versus a stair-step target..... 8

Figure 8. Gate Profiles from Camera 1 (red) and Camera 2 (blue) 10

Figure 9. Typical single camera 100 frame average image from Makai Pier experiment..... 12

Figure 10. Shearography SERDP test configuration. 12

Figure 11. Acoustic source (speaker) facing the target area..... 13

Figure 12. The shearography transmitter and receiver. 13

Figure 13. Series of shearograms with increasing phase offset..... 14

Figure 14. Makai Pier experimental setup. 16

Figure 15. Deployed simulated shell and background plate within wave-dampening device..... 17

Figure 16. Target orientation 1 for shearography field test. 18

Figure 17. Target orientation 2 for shearography field test. 18

Figure 18. Grey scale images of each spectral band from the MSI sensor. I..... 20

Figure 19. Output from the Canny edge detection algorithm 21

Figure 20. Top-down view of a final REVEAL elevation map. 23

Figure 21. Profile (side) view of the ratio output. 23

Figure 22. Shearogram of Shell, Depth = 1.5”, Freq. = 90 Hz, Shear = Vert, Speaker = 0 deg. (Exper. 100323c_Run06_0304)..... 24

Figure 23. Shearogram of Shell, Depth = 1.5”, Freq. = 100 Hz, Shear = Hor, Speaker = 0 deg. (Exper. 100323f_Run07_0506) 24

Figure 24. Shearogram of Shell, Depth = 1.5”, Freq. = 110 Hz, Shear = -45, Speaker = +45 deg. (Exper. 100324b_Run08_1011)..... 24

Figure 25. Shearogram of Shell, Depth = 1.5”, Freq. = 120 Hz, Shear = +45, Speaker = +45. (Exper. 100324d_Run09_0405)..... 24

Figure 27. Shearogram of Shell, Depth = 3”, Freq. = 110 Hz, Shear = Hor, Speaker = 0 deg. (Exper. 100324m_Run08_0203)..... 25

Figure 28. Shearogram of Shell, Depth = 3”, Freq. = 110 Hz, Shear = -45, Speaker = +45 deg. (Exper. 100324r_Run08_0203) 25

Figure 29. Shearogram of Shell, Depth = 3”, Freq. = 110 Hz, Shear = +45, Speaker = +45 deg. (Exper. 100324t_Run08_0102)..... 25

Figure 30. Shearogram of Shell, Depth = 3”, Freq. = 110 Hz, Shear = -45, Speaker = -45 deg. (Exper. 100324x_Run08_0809)..... 25

List of Acronyms

Acronym	Content
CDOM	Colored Dissolved Organic Matter
DoD	Department of Defense
FPA	Focal Plane Array
LIDAR	LIGHT Detection And Ranging
MSI	Multi-Spectral Imagery
NIR	Near InfraRed
ONR	Office of Naval Research
REVEAL	Rapid Efficient Volumetrically-Enabled Lidar
SAMSS	Synoptic Airborne Multi-Sensor System
UXO	Unexploded ordnance
VNIR	Visible to Near Infrared

1.0 Abstract

Many active and former military installations have ranges and training areas that include adjacent water environments that pose technical challenges for cleanup of unexploded ordnance (UXO). This SERDP project was aimed at testing advanced technologies, originally developed for mine detection under the Synoptic Airborne Multi-Sensor System (SAMSS) program, for underwater UXO detection. Multiple technologies were investigated during the project, including:

- multispectral imaging
- REVEAL (Rapid Efficient Volumetrically-Enabled Lidar) and
- lidar shearography.

Of the three technologies, two (MSI imagery and REVEAL lidar) were tested simultaneously from the Makai Pier in Oahu against the same target fields. However, while results from each of the three technologies were promising, more work needs to be done to ensure a fused “synoptic” solution can be achieved.

2.0 Objective

The objective of the proposed research project was to adapt and exploit the capability of a synoptic sensor system, developed under the auspices of a land mine detection program, to detect underwater UXO, including ordnance buried beneath the seabed. This system is termed “synoptic” because it synergistically integrates three simultaneous distinct modes of passive and active sensing with knowledge-based information to create a detection system that is expected to be, in principle, orders of magnitude more capable than any one sensor.

3.0 Background

Many active and former military installations have ranges and training areas that include adjacent water environments such as ponds, lakes, rivers, estuaries, and coastal ocean areas. Most munitions operate properly, but historical records indicate that up to 10% of all munitions fail to detonate as designed¹. Due to the technical challenges created by the water medium, UXO detection technologies and, therefore, the cleanup of these sites have lagged technologies and cleanup on land, especially with respect to ordnance buried beneath the seabed. Although difficult, cleanup of underwater sites is among DoD priorities for environmental programs.²

Ordnance can take many forms but is often artillery shells that are buried to varying depths beneath the seabed. Underwater UXO sites may consist of various water salinity/depths and bottom compositions, littered with buried and unburied unexploded ordnance as well as debris fields arrayed according to patterns that developed by the long term use of the training sites (target areas, extent of flight, etc.). In deeper water, most UXO will be found on the bottom or buried just below the seabed, where the bottom is composed of deep layers of mud or fine silt, gravitational burial may be expected. Where the seafloor has little sediment, the UXOs are often bio-fouled with corals and algae, making them appear similar in color to the bottom (Figure 1).

Typical ordnance at underwater sites can take many shapes and sizes³, and reside in a variety of environmental conditions. Ordnance landing in shallow water may bury on impact to varying depths, depending on angle of impact; soil type; speed of aircraft and impact; height of release and shape. In deeper water most UXO will be found on the bottom or buried just below the

seabed due to scouring effects caused by hydraulic forces. Where the bottom is composed of deep layers of mud or fine silt, gravitational burial may be expected. In many cases, burial can be modeled and predicted with some accuracy using tools such as the “adapted” VORTEX model⁴ and that knowledge exploited. Underwater sites, therefore, may consist of various water salinity, depths and bottom compositions, littered with buried and unburied unexploded ordnance as well as debris fields arrayed according to patterns that developed by the long term use of the training sites (target areas, extent of flight, etc.).



Figure 1. Examples of UXO munitions, bio-fouled and encrusted with corals and algae.

3.1 Existing Detection Methods

What is needed is a fast, efficient means for detecting underwater UXO. Examples of existing technologies and their shortcomings include:

- Synthetic-aperture ground-penetrating radar is of little use in estuarine and coastal soils, (except in very shallow freshwater sites) due to the electrical conductivity of saltwater, as is shown in Figure 2;
- Magnetometers have poor discrimination capability, very limited coverage rate and suffer from high false alarms, although some recent significant advances have been made on land using magnetometer and electromagnetic induction combinations⁵;
- Sonar systems, especially high resolution side-scan sonars have good coverage rates and discrimination of proud objects on the bottom, but are not generally usable in the very shallow inshore areas, especially where there is active surf, and do not typically penetrate the bottom; and
- Acoustic sub-bottom profilers tend to be cumbersome low frequency systems with large arrays and also are limited to deeper water depths and have low coverage rates.

It should also be noted that traditional seismic survey techniques using geophones have been proposed and recently tried with mixed success for underwater UXO detection.⁶ Several past approaches have involved fusion of two or more of these technologies with limited tactical/operational success.⁷

3.2 Optical UXO Detection

Detection of partially buried or proud underwater UXO is possible in waters where backscattered light from the seafloor has a higher intensity than backscatter from the water column. While pure water does scatter and attenuates light, the optical properties of natural waters are dominated by suspended sediment, colored dissolved organic matter (CDOM) and phytoplankton. Seawater

and its constituents exponentially attenuate (following Beer’s Law) light via absorption, as well as via scattering in all directions. The light backscattered back towards the viewer is the main component of the upwelling-light signal strength and shape in deep water. In shallow water, seafloor backscatter can also be a major contributor to the upwelling light, with the apparent reflectance of the bottom being modulated by attenuation and scattering in the overlying water – the scattering also blurs bottom features and causes apparent color shifts at feature edges. In clear tropical waters with little chlorophyll, CDOM and suspended sediment, visible wavelengths will penetrate further than in turbid coastal waters near river outflows or after rainstorms. Therefore the utility of visible wavebands for ordnance detection depends on the water type, recent weather, and the coastal environment. For purposes of conceptual employment, typical ordnance may be expected to be detected to a nominal water depth of approximately six meters.

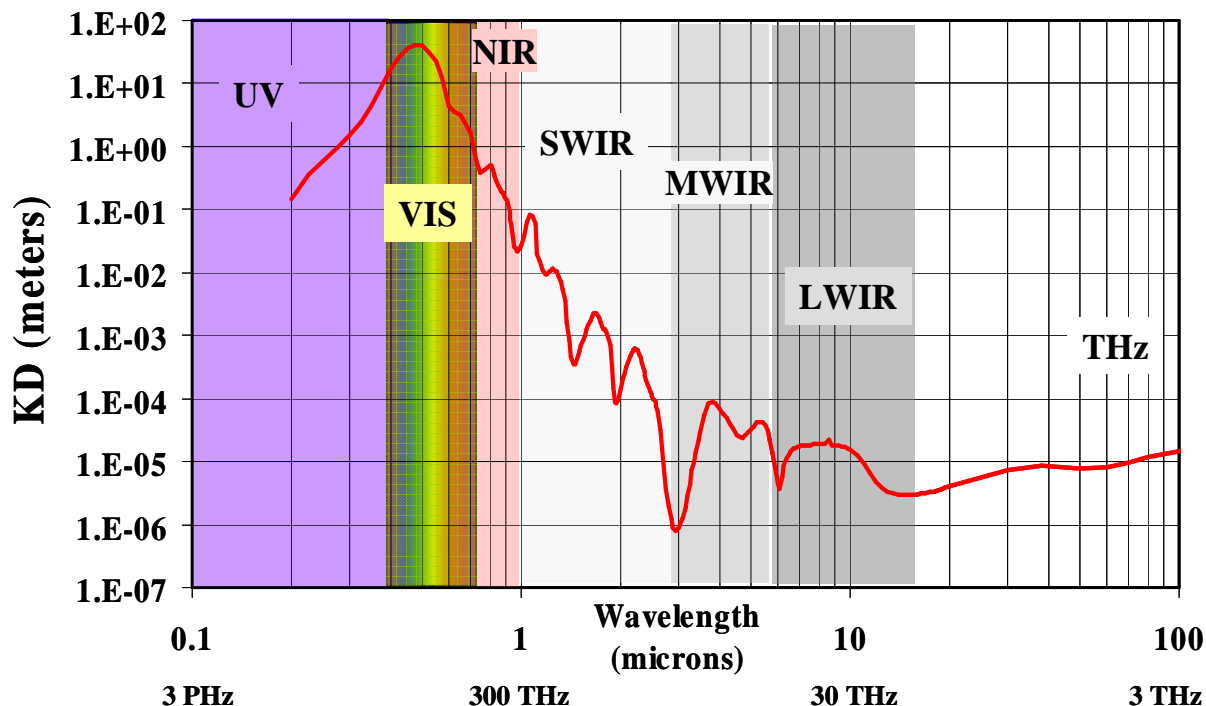


Figure 2. Wavelength-dependent attenuation of electromagnetic radiation in pure seawater. KD is the distance at which light attenuates by a factor of 1/e. For wavelengths longer than the near-infrared (NIR), penetration of radiation in seawater is negligible.

Despite the difficulties of imaging through water, the differential attenuation of various wavelengths of light in water (Figure 3) can be exploited to retrieve many types of information about ordnance and the environment. Knowledge of the water type can be combined with knowledge of the spectral reflectance of bottom constituents (Figure 4) to infer both water types and bottom composition from remotely-sensed light spectra. For the ONR-funded system, six bands were chosen to cover major spectral regions of variability and capture information that can be used to distinguish different types of objects or bottom composition. These bands constituted a Visible-NIR (VNIR) multispectral suite including 5 bands in the visible spectrum (400nm – 700 nm) and one in the near-infrared (above 700 nm). The utility of the near-infrared (NIR) band derives largely from the fact that infrared radiation does not penetrate seawater deeply. Thus, any strong signal in the infrared must arise from surface objects or from reflections of above-surface

objects (such as clouds). This allows improved discrimination of surface clutter (such as foam and glint), and detection of floating objects.

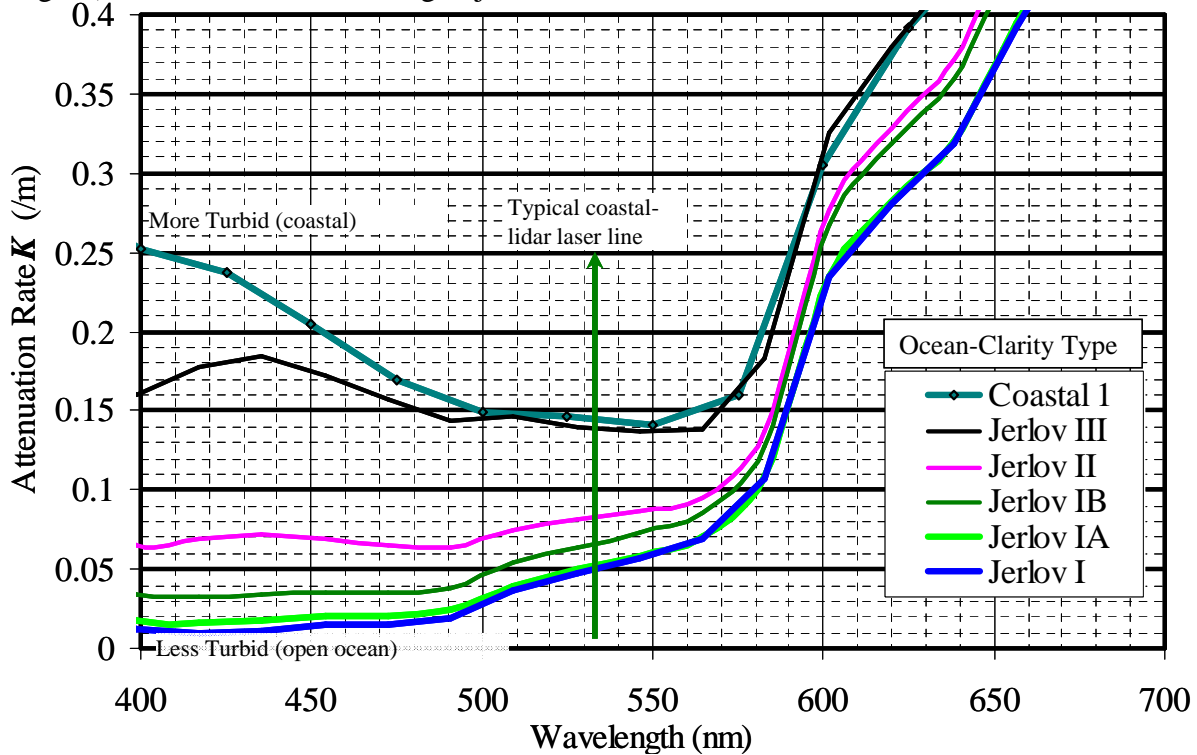


Figure 3. Attenuation rates versus wavelength for various water turbidity types (classification from N.G. Jerlov⁸)

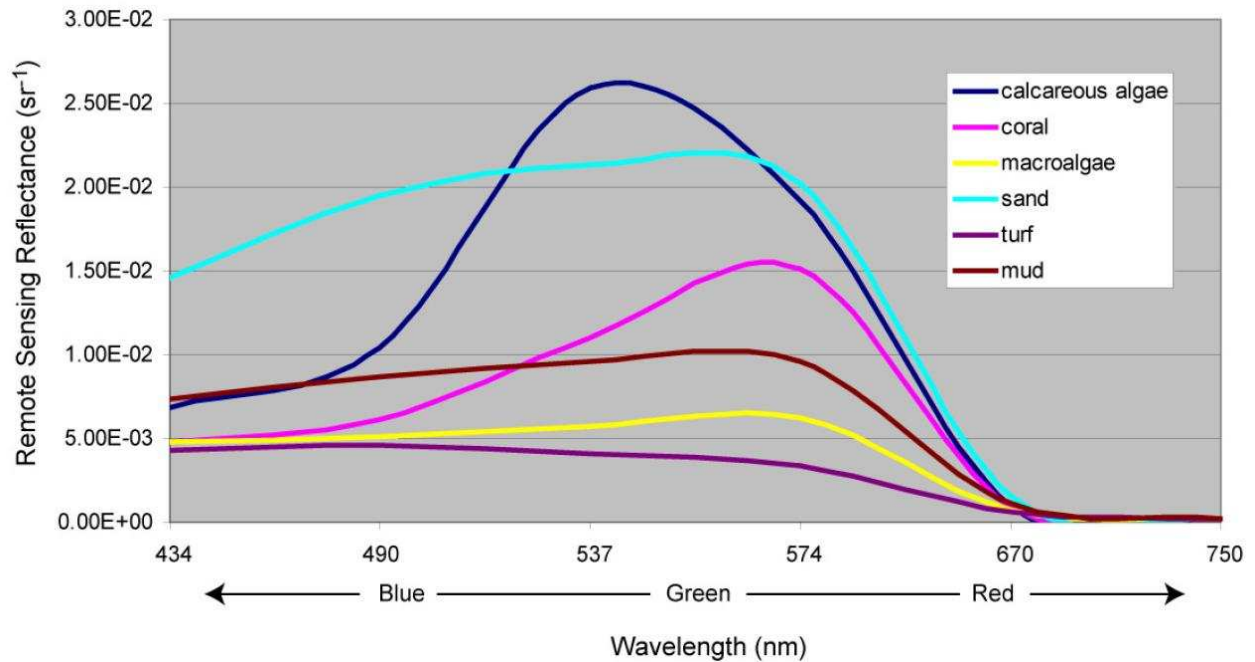


Figure 4. Remote-sensing reflectance spectra of different bottom types at 3 meter depth in tropical waters. All of the bottom types retain sufficient spectral information to allow for discrimination and classification.

The utility of multiple well-chosen imaging bands (As opposed to simple 3-band color imaging) arises from the fact that ordnance may be painted with a variety of color schemes, or develop a weathered or bio-fouled coloration after some time in the water (See Figure 1). Therefore ordnance may have no characteristic spectrum or it may take on the spectrum of the unique growth naturally selected to adhere to its case (frequently in concentrations and spectral properties that are *not* typical of the background). The fact that there is upwelling light in the blue and green wavelengths allows one to use spectral anomaly detection routines to find objects that do not match the natural background in color or shape. In some cases, UXO will have been submerged for many years and will have accumulated a thick covering of encrusting flora and fauna, making it spectrally identical to the seafloor. In this case, it would be necessary to use an algorithm that detects the overall physical shape of the UXO as opposed to the spectral signature.

3.3 Optical-Acoustic UXO Detection

Shearography is based on optical interferometry and takes advantage of the long coherence length of laser light to form interference patterns of the back-scattered light from the target area with light from a reference beam. If the path difference between the two arms of the interferometer is less than the coherence length of the light source, the beams are summed taking into account the vector nature – direction, amplitude and phase – of the electric fields, rather than simply summing the intensity of the light waves. This vector sum is the basis for the bright and dark fringes of interferograms which indicate constructive and destructive interference, respectively.

For shearography the source of the “reference” wavefront is light backscattered from the target itself, but displaced relative to the test wavefront by a given distance known as the shear distance. As the distance from the sensor platform to the target area changes, the path lengths of both the test and reference arms in the interferometer change at nominally the same rate since the beams are nearly common path. Therefore, to first order, the resulting interference pattern is unaltered. This common-path characteristic is the reason shearography is less sensitive to sensor platform motion than other techniques.

Shearography operates by detecting differences between two successive (short exposure) interferograms of the vibrating target surface. However, since the reference wavefront is derived from neighboring points on the target surface, the resultant map, known as a shearogram, displays fringes that are to first approximation contours of equal *change in the surface slope* between the two exposures. Specifically, it is the component of surface slope along the shear direction that is detected. The fringe contours are spaced at intervals equal to slope changes of $\pm \lambda / 2 D_{\text{shear}}$, where λ is the laser wavelength and D_{shear} is the shear distance. Since the fringe spacing is inversely proportional to the shear distance, the sensitivity of the technique can be adjusted by altering the amount of shear⁹. Increasing the shear increases sensitivity to target slope changes.

4.0 Materials and Methods

The synoptic sensor suite was comprised of three main components, tested separately and characterized as to their capabilities to detect buried ordnance, unburied ordnance, bottom features, and environmental parameters (**Table II**). Each sensor exploited a distinct aspect of the

physics of light propagation in marine environments. The common detection methodology is optical, since the sensors are ultimately intended for airborne use. (For maritime mine countermeasures applications, optical methods are the only means even *theoretically* capable of detection through the air-water interface at tactically-useful search rates, and with sufficient resolution to discriminate ordnance from biologics and non-mine debris.) By combining multiple independent methods of detection, a suite of sensors can achieve detection performance far superior to any one sensor alone. Operated together, as in Figure 5, they may provide enhanced detection probabilities and orders of magnitude reduction of false alarms. The sensors are discussed in more detail in following subsections.

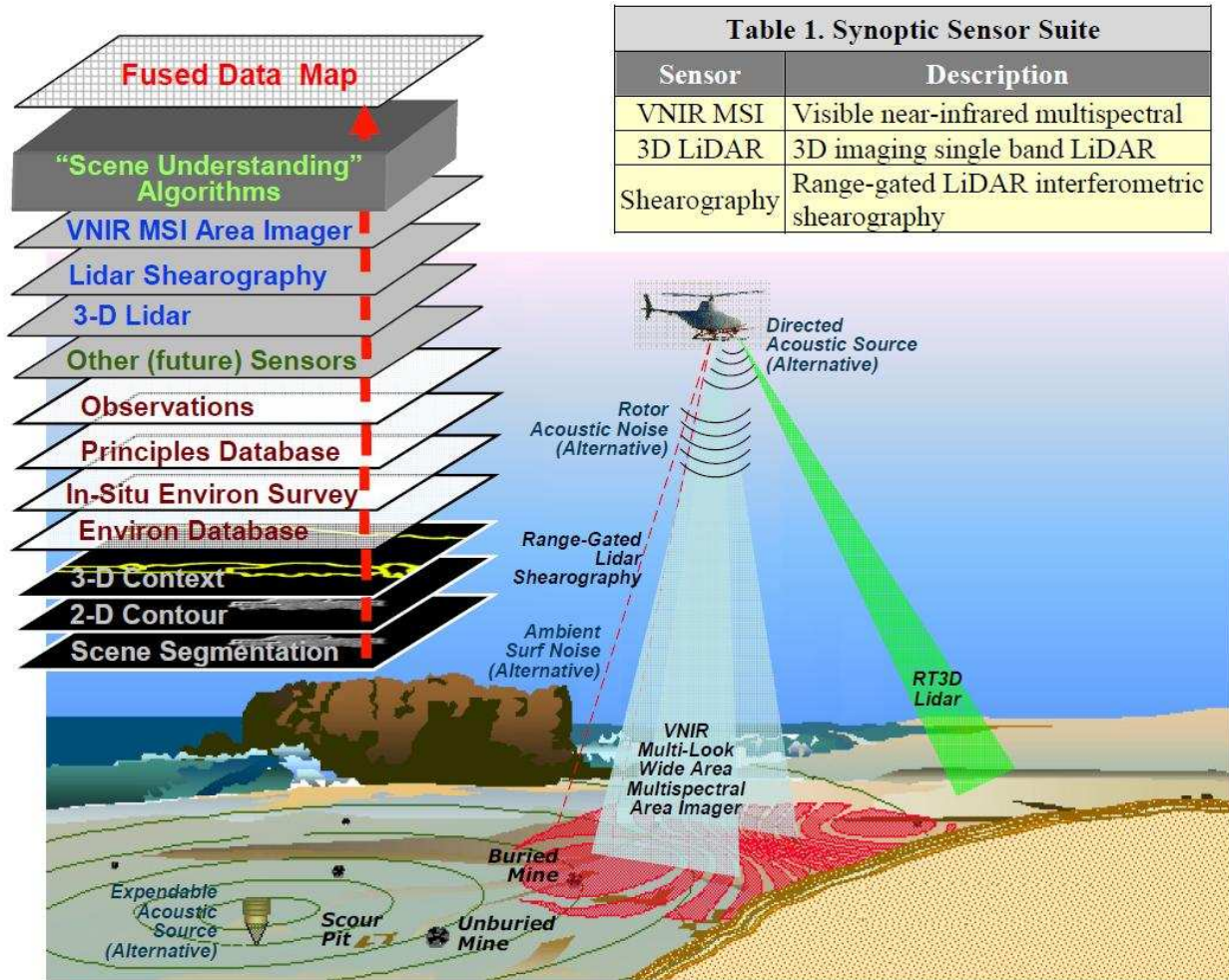


Figure 5. Schematic overview of the mine-detection system for the SAMSS project.

Table II. Summary of Phenomenology Studies

	Sensor	Proud UXO	Buried UXO	Scour Pits	Background Variability
Water Tank or Field (Pierside)	VNIR MSI	Spectrum		Spectrum	Spectrum
	REVEAL	Shape		Shape	Features
	Shearography	Speckle Signature	Speckle Signature	Speckle Signature	Vibration Signature

4.1 Multispectral Imagery

The multispectral imager (MSI) used in this study was a 6-band, compact imager designed for surf-zone mine detection for the Office of Naval Research (ONR). The 6-pack is a high-performance miniature multispectral area imaging sensor designed for turreted and small-UAV configurations. The 6-pack technical features include: 1000 x 1000 pixel resolution, high quantum efficiency Focal Plane Array (FPA), independent band-tailored optics, configurable VNIR Spectral Coverage, and camera-link imaging interface.

The MSI method offers the potential for seeing through the glint and foam clutter on the sea surface. This is due to the framing nature of the MSI system, in that multiple ‘looks’ of scene are collected over a short time period, and can be merged to enhance system performance, as shown in Figure 6. This enables at least one good look at the targets of interest during the typical 6-second period for which a given target is in the system field of view during overflight. (Stationary systems can take advantage of more looks.) Further gains are obtained by removing glints and foam in each multi-band frame before the merge, and running spectral-discrimination algorithms on merged de-glinted image frames.

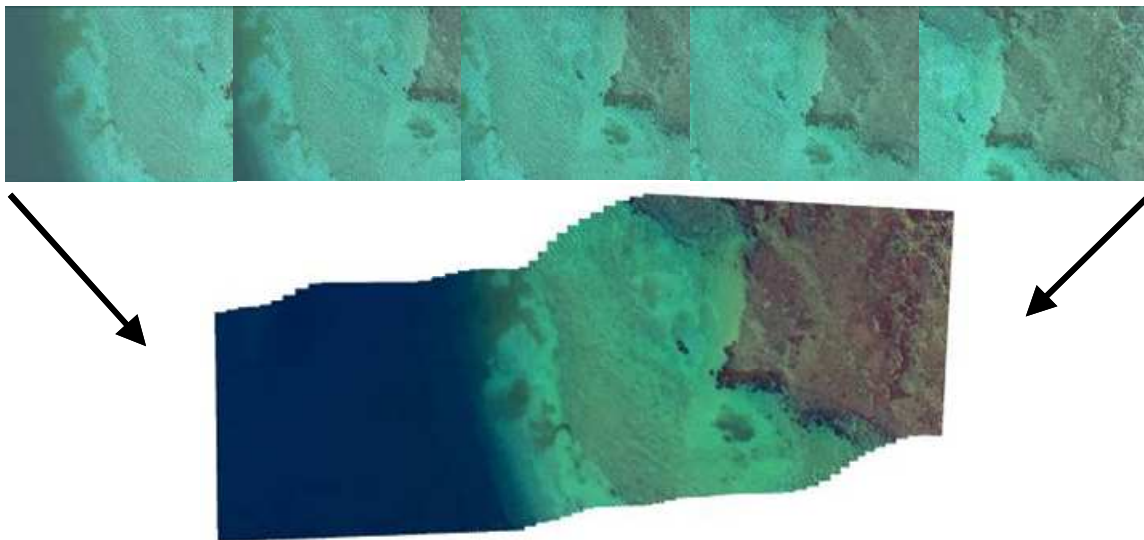


Figure 6. Demonstration of glint and foam removal due to the merging of multiple, overlapping image frames from the 6-pack MSI.

For the SERDP program, the MSI imagery was split into individual spectral bands, with each band analyzed independently. Rather than spectral discrimination of targets using the six-band imagery, we chose to focus on edge detection to identify the straight (i.e., man-made) edges in the images. The Canny method finds edges by looking for local maxima of the gradient of a vector of interest. The gradient is calculated using the derivative of a Gaussian filter. The method uses two thresholds, to detect strong and weak edges, and includes the weak edges in the output only if they are connected to strong edges. This method is therefore less likely than the others to be fooled by noise, and more likely to detect true weak edges. The edge detection was implemented using the standard Matlab Canny edge-detection routine.

4.2 REVEAL

The REVEAL imaging method offers the potential for observing the shape of ordnance on the bottom, indicators of ordnance such as scour pits, and bottom features. Because REVEAL is implemented with a range-gated ICMOS (Intensified CMOS) camera, the large array size (1024 x 773) provides detailed information on the 3D shape of objects. The REVEAL resolution capability is illustrated in Figure 7. REVEAL range maps are insensitive to non-uniform target reflectance and inhomogeneity of the illumination source, though very dark objects yield noisy range images. In the example shown in Figure 7, the 1.3-inch (3 cm) steps are clearly defined in the REVEAL image, while they are not distinguishable in the conventional lidar picture. For a conventional imaging lidar to achieve similar range resolution would require digitization at a sampling rate exceeding 10 GHz, beyond the capabilities of current technology.

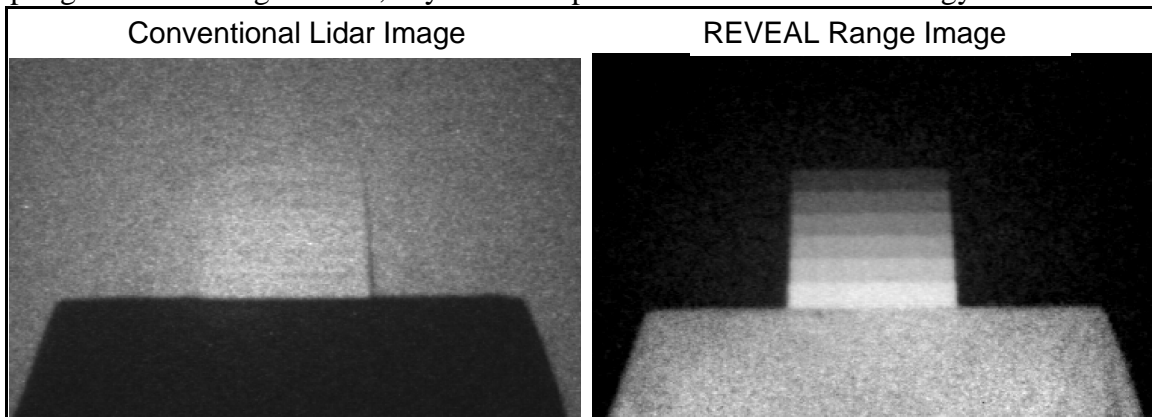


Figure 7. REVEAL operation in laboratory versus a stair-step target on felt-covered tabletop against a white wall. Left: conventional lidar image, showing features dominated by reflectance variations. Right: REVEAL imaging range map – lighter is closer, darker is further away.

The REVEAL system employs a range-gated LiDAR, which registers all pixels simultaneously, thereby reducing image distortion, software complexity, and improving energy efficiency enabling deeper penetration. The REVEAL technique collects fine-resolution in all three spatial dimensions without requiring high speed temporal sampling (GHz or faster). REVEAL distances are computed from pairs of range-gated lidar returns collected with gates much wider than the size of the object being imaged. Despite the thickness of the range gates, REVEAL achieves precise range resolution by exploiting the temporal *shape* of the gate- the way the gates ramp up and down as the camera is turned on and off, using the nonlinear slope $r(t)$ of the upramps and downramps of the gain curve. A pair of images collected to place the target at different places on the ramps is processed to separate reflectance from range and render an image of ranges to target across the entire image.

To select the best delays for REVEAL computations, proceed as follows.

1. Measure and plot a gain profile.
2. Convert the target height h to delay time τ through $\tau = (2nh/c)$, where n is the index of refraction, and c is the speed of light in vacuum.
3. Find the point of maximum slope for each ramp, and center an interval of width τ around this point.

4. If the gain profile was measured at the furthest distance of the target, then use the end of each interval that has the shortest delay time.

4.2.1 Gate Profile Generation

The following sequence of data processing steps assumes knowledge of how to choose the correct time values for the gate profile for the laser. In addition, depending on the experiment environment, one can choose a 10ns, 15ns, or 20ns laser pulse width. For shallow water it is desirable to use the shortest pulse width possible that produces linear regions on the “up ramp” and “down ramp.” Most of our experiments used a pulse width of 15ns, which corresponds to a gate thickness of 7.5 feet in air, and 5.6 feet in water.

We collected 100 frames per time slice, therefore each raw file contains 100 frames sampled at 30 Hz. Typical time values used for the laboratory setup were in the range of 50 – 70ns, with samples taken at 1ns intervals. To create a plot of the Gate Profile over time, we choose a region of interest within the frame, typically a small rectangle within the center of the image frame. The gate profile across different regions of the image are not identical. Therefore it was important to select a ROI representative of the target and at a similar field of depth. The Gate Profiles were created in Excel.

In the laboratory the measured gate profiles for Camera 1 and Camera 2 were nearly identical, and therefore the analysis methods were designed with that assumption. In the Makai Pier experiment however, it was discovered that the two gate cameras had gate profiles shifted by about 2ns. (Figure 8). It was not determined what caused this shift: the electronics, environmental conditions, or the air to water differences.

Because the gate profile is used as the empirical calibration data for producing a range map, it is important that this data be as accurate as possible. This means imaging points in time spanning 35 – 45 ns to produce a gate profile curve.

4.2.2 Ratio Image File Generation

Once the gate profile is calculated the next step is to average each of the 100 frames in each data file into a single image. Then the average image from the “down” portion of the gate profile is divided by the average image from the “up” portion of the gate profile (Eqn (2)). This stage requires some experience on selecting the best image pairs that will create the optimal 3D image. In general if we have 5 images on the up ramp and 5 images collected on the down ramp, there are $5*5=25$ possible pairings of up/down images. Of these 25 image ratio combinations some combinations will produce better results with regard to noise, illumination, and SNR.

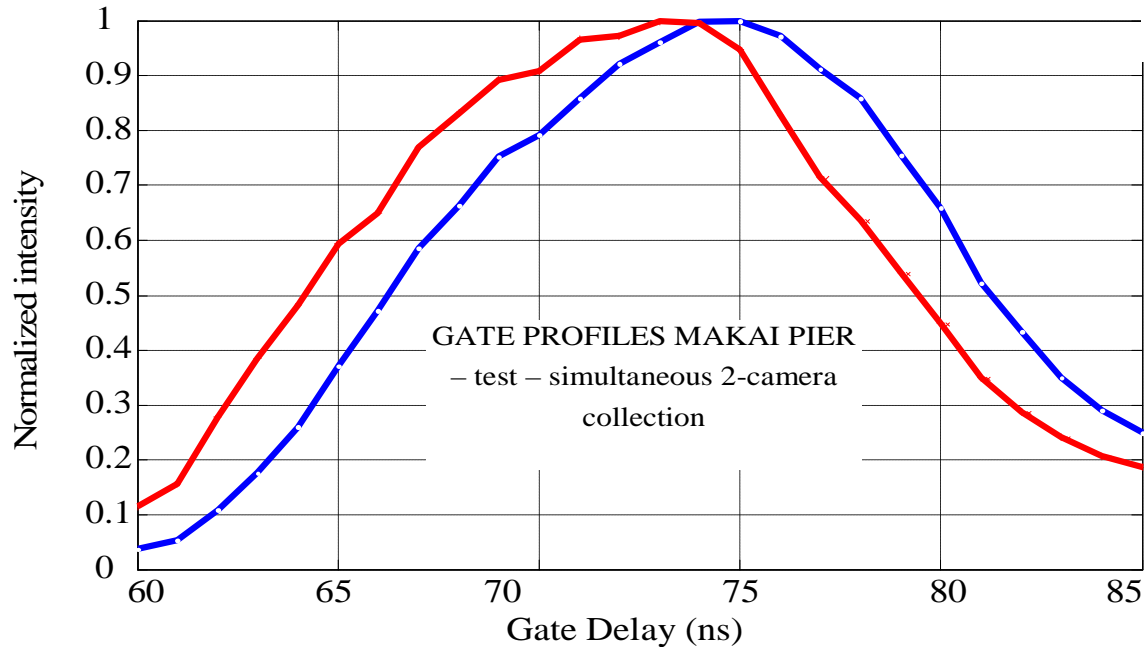


Figure 8. Gate Profiles from Camera 1 (red) and Camera 2 (blue) from the Makai Pier data collect.

4.2.3 Distance Calibrated Relief Image Generation

The next step in the REVEAL processing is to convert the best ratio image products created in Section 4.2.2 into distance (in cm). The interpolation of ratio-to-distance values is calculated *in situ* by calibration imagery taken at the beginning of the field exercise and the known water depth (Eqn (3)). The initial conversion proved to be too noisy to handle effectively, and therefore was spatially smoothed using a contra-harmonic mean filter. (See Gonzalez and Woods, *Digital Image Processing*, Third Edition). The filters were implemented with the MATLAB function `ordfilt2`, a 2-D order-statistic filtering function. Once the distance calibrated image is spatially filtered, the `surf` function in MATLAB can be used to create 3D surfaces with this 2D matrix.

4.2.4 One Camera LIDAR

The first data collects in the program utilized only one camera (receiver) in the REVEAL set-up, using two sequential images for the REVEAL 3-dimensional images can be created using a “gate profile” function to create a relationship between intensity ratio and distance. The intensity ratio is the ratio between two co-located pixels imaged at different times. This output distance, or relief, corresponds to a 3D shape of the scene.

The returning light from a scene is a convolution between the laser pulse, the scene reflectance, and the gain profile of the camera intensifier. To create this distance map of an object or scene, we need: 1) a gate profile, and 2) two images from within this gate profile time range.

4.2.5 Two camera LIDAR

Adding a second camera allows the ability to rapidly sample an underwater scene, with two images sampled within a few nanoseconds. This rapid sampling allows the system to operate even in the presence of turbulence and distortions on the water surface. Essentially one “up ramp” image is collected by Camera 1, and one “downramp” image is collected by Camera 2 using the same laser pulse.

Adding a second camera adds several new analysis complexities in that a) the two images must now be coregistered and b) two gate profiles must now be collected: one for Camera 1 and one for Camera 2. The procedure used when working with two cameras is as follows:

1. Collect Dark File
2. Collect Gate Profile for Cameras 1 and 2
3. Calculate the Gate Profile for Cameras 1 and 2
4. Coregister the imagery from the two cameras
5. Collect Imagery over the targets
6. Create Range Map
7. Convert ratio files to depth images (in cm)

4.2.6 Dynamic Range and Glint

One of the significant challenges with the REVEAL data was the tendency for closer objects to be much brighter than distant objects (Figure 9). This artifact became significant when adjusting images and color maps for optimal viewing in that the optimal dynamic range of interest for the target is often a tiny fraction of the full range. For example, the majority of pixels for the shell and disk in Figure 9 have a digital number of just 0.01 - 0.05 out of the 0.0 to 1.0 digital number range for the entire image. (The camera system samples at 10 bits depth.)

4.3 Shearography

Shearography is a high-sensitivity speckle-interferometric technique that is used to observe and measure the spatial structure of the displacements of an object surface. Object surface motion is typically induced by application of an acoustic or mechanical forcing function. Shearography takes advantage of the fact that a surface whose vertical roughness scale is greater than the wavelength of the laser light illuminating it will produce a visible speckle pattern superimposed on the image of the surface. The speckle pattern has the appearance of spatial white noise. When viewed through an imaging shearing interferometer, the speckle pattern serves as a random spatial carrier of information about the state of the object surface. Typically, buried objects are displayed as anomalous images within this speckle pattern. In addition objects such as buried ordnance may exhibit, within the temporal data, a resonant “ringing” effect in the form of separate “waves” emanating from the object.

4.3.1 System Configuration

The general layout of the equipment is depicted in Figure 10. To provide a near-nadir view of the target area, the laser source and shearography sensor breadboard tilted up toward a fold mirror. The fold mirror was mounted and secured onto a structure assembly. Under the mirror was a tub filled with sand. The mirror dimensions were 38 inches x 26 inches. The tub dimensions were 72 inch diameter and 24 inch depth.



The system control electronics including the computer with framegrabber, laser controller, and trigger delay generator were housed in an electronics rack.

Figure 9. Typical single camera 100 frame average image from Makai Pier experiment. Target is the shell on a flat disk. At the top of the image, glint is evident from the top white pipe and the water surface.

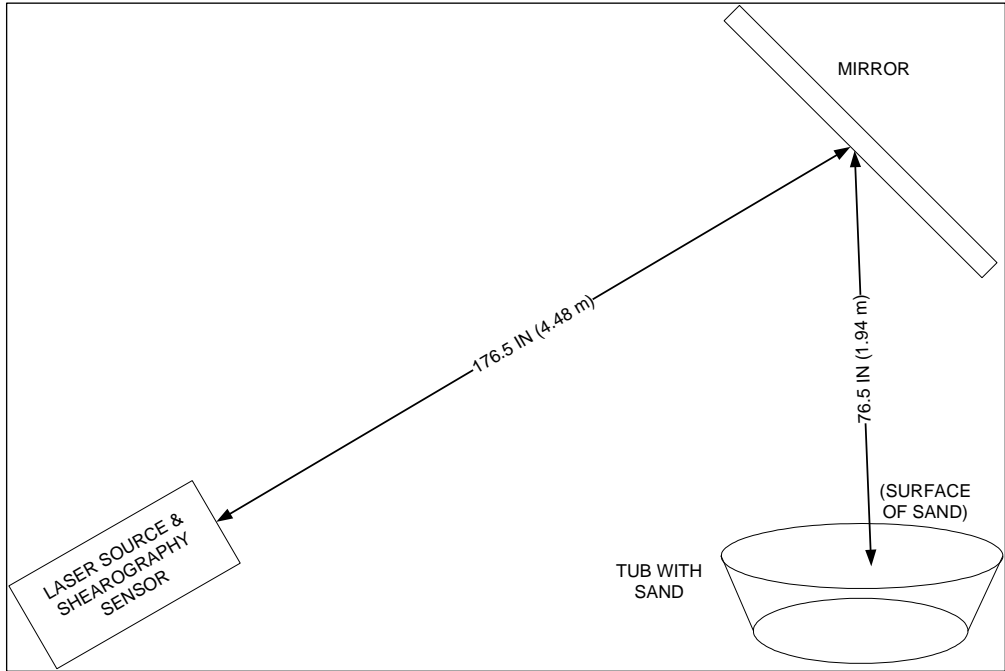


Figure 10. Shearography SERDP test configuration.

The acoustic driver (speaker), MTX Audio model TP1200, rested on a cart facing downward toward the target area on the sand (Figure 11). The speaker grill was approximately 40 inches from the target area on the sand.

Finally, the shearography transmitter and receiver are mounted together on a common platform (Figure 12).



Figure 11. Acoustic source (speaker) facing the target area.

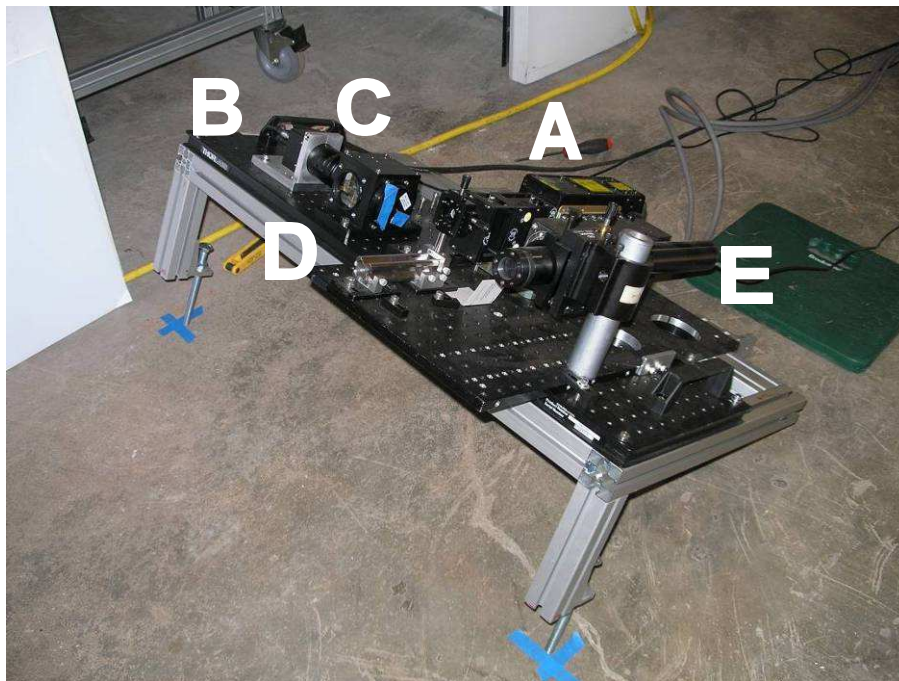


Figure 12. The shearography transmitter and receive mounted on the inclined breadboard plate. A: laser; B: CCD camera; C: lens; D: Michelson shearing cube; E: alignment laser.

4.3.2 Shearography System Operation

The basic mode of operation of the system is to insonify the target zone with a single frequency sound wave in the range from 40 Hz to 500 Hz and trigger a camera exposure and laser pulse at the peak and at the valley of target (sand) surface motion. Ideally, the triggers would occur within a single cycle of the acoustic wave. However, this timing would require the laser and camera to operate at rates from 100 to 600 Hz. Since the camera used for the breadboard sensor was limited to frame rates less than 14 Hz (71.4 millisecond frame time), the two exposures comprising one shearogram were spaced in time by an integer-plus-one-half acoustic periods to arrive at a delay of 71.4 ms or greater. The control program calculated the minimum number of acoustic cycles required for this delay. Furthermore, since the phase offset between the acoustic signal and the target surface motion was not known a priori, the target was sampled at each frequency with a series of phase offsets. A series of twelve exposures, evenly spaced in time by $(m + 1/2 + 1/24)$ acoustic periods, where m is an integer, were acquired. Successive images were paired to form a series of shearograms with nearly 180° ($360^\circ \times 13/24$) phase difference and phase offsets incremented by 15° ($360^\circ / 24$). Figure 13 shows every other shearogram of a cylindrical test target from such a series. The peak in the number of fringes occurs at 30° offset, while the null occurs 90° degrees later at 120° offset.

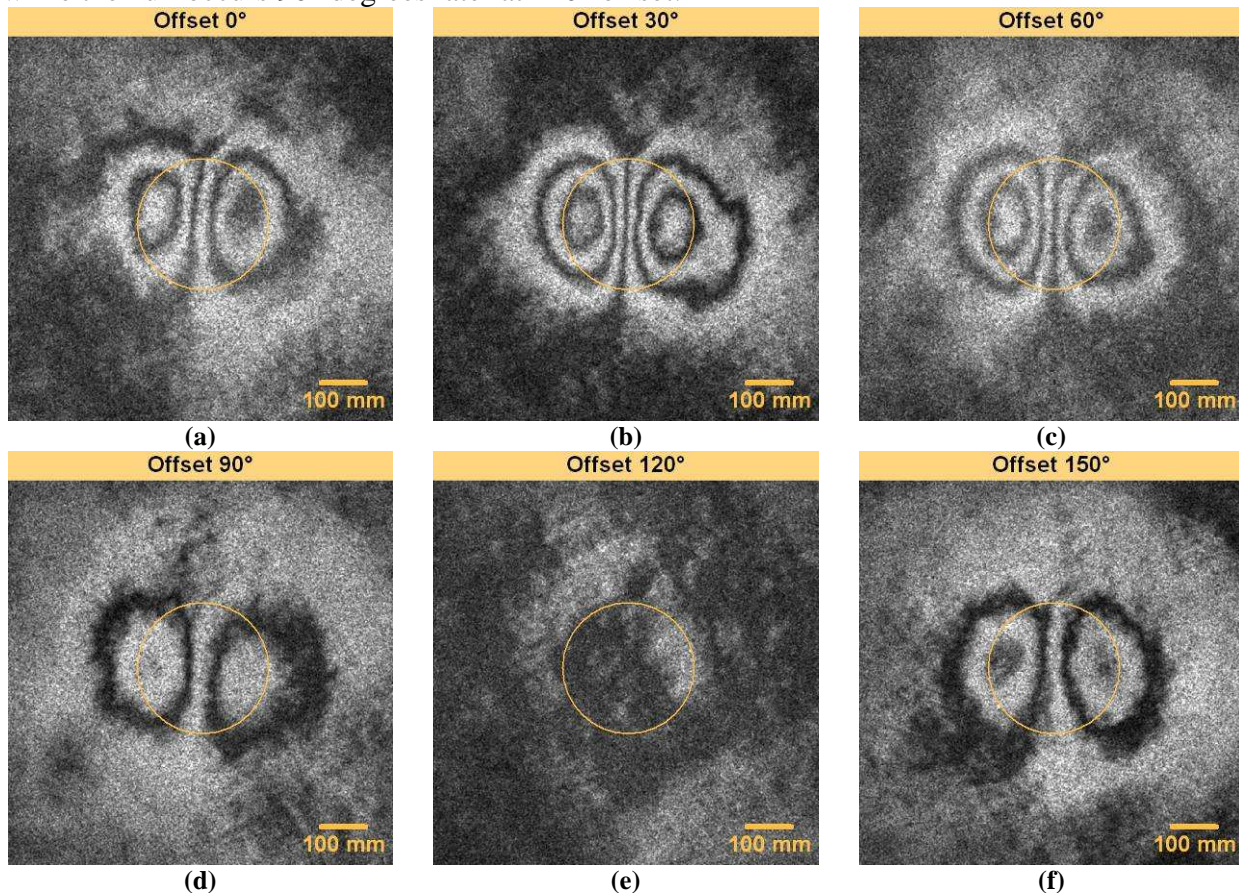


Figure 13. Series of shearograms with increasing phase offset between the sinusoidal acoustic signal and the first laser shot. The maximum surface motion (b) occurs near 30° offset and the minimum (e) occurs 90° later and roughly 120° offset.

The shearography transmitter consists of a pulsed, frequency-doubled Nd:YAG laser, beam diverging optics and downward pointing fold mirror. A single -11.4mm focal length lens produces a beam divergence of 10° FWHM. Some of the key specifications Big Sky Centurion laser are:

- Wavelength 532 nm,
- Energy per pulse 20 mJ,
- Maximum pulse rate 100 Hz,

The shearography receiver is configured as a Michelson interferometer (D in Figure 12) followed by a camera lens and CCD imager. The Michelson has a 50 mm beamsplitting cube and two mirrors equally spaced from the cube, which are tilted with respect to one another to set the image shear distance. For the experiments of this test, the shear distance was set to 55 ± 5 mm measured at the target surface, but at various orientations with respect to the target axis. The 75 mm focal length lens and 1600 x 1200 pixel camera yielded a field-of-view equal to 1.02 x 0.77 m. The scale used was 0.639 mm per pixel. The tolerance on the parallelism of the target surface and shearography platform in the direction of shear was set to $\pm 1^\circ$.

4.3.3 Data Processing and Analysis

The basic process of computing a shearogram from the raw camera images is rather straightforward for shearography with a static platform. The shearogram is calculated by taking the absolute value of the difference of two sequential CCD exposures on a pixel-by-pixel basis. The resulting shearogram is convolved with a 7x7 Gaussian low-pass filter kernel to improve the plotting and viewing of the shearogram fringes. If the laser illumination remains constant for the two exposures, the above processing steps are sufficient for calculating shearograms from the raw images. However, the mode structure of the Nd:YAG laser used in this experiment changes slightly from shot to shot. The variations are on the order of 10% of the base Gaussian-beam intensity with transverse dimensions on the order of 5% of the far-field beam diameter. Without correction, the variations in target illumination cause spurious patterns in the shearogram image which mask the fringe patterns from the deformations of the target. The effects of the laser mode fluctuations can be reduced significantly by normalizing the two raw images prior to calculating the shearogram. The image normalization is accomplished by dividing, on a pixel-by-pixel basis, each raw image by its low-pass filtered image which is calculated using 21x21 pixel averaging kernel.

As a last step, emplacement image outlines are added to each shearogram, as a guide to the eye.

4.4 Field Experiment Set-Up

There were two distinct field experiments to test the feasibility of detecting underwater UXO using the above outlined techniques. Each is described in detail below.

4.4.1 Makai Pier

On January 11, 2010 a data collection experiment was conducted at Makai Pier, off the Eastern point of the island of Oahu. The goal of this experiment was to test the detection capability of the optical MSI sensor and the REVEAL laser technology. The experiment was conducted over a several hour period in a water depth of approximately 5 ft. The targets were imaged through a wave-dampening plexiglass enclosure, to remove, in this initial experiment, wave effects from the LIDAR imagery (Figure 14).

Prior to embarking on the field work, the two REVEAL cameras were calibrated and their gate profiles curves calculated via a series of laboratory measurements (see Section 4.2.1). These initial profile curves were used to pre-seed the *in situ* calibration necessarily to account for the actual water depth and sample profile in the field.

The first step in the field experiment was to perform an *in situ* calibration of the two camera REVEAL set-up. A white calibration disk was deployed on the sea floor, above which was suspended the wave-dampening apparatus (Figure 14). The calibration panel was then imaged with the REVEAL



system, the gate profile curves were calculated, and the results used in all subsequent analysis.

Figure 14. Makai Pier experimental setup. Note the mobile laser lab on the pier surface, the wave dampening plexiglass device deployed in the water, and the white calibration panel on the seafloor.

In addition, the white calibration panel was imaged by the six-camera MSI system to provide *in situ* brightness correction and spatial correlation with the REVEAL imagery.

The next step in the experiment involved placing a grey cover over

the white calibration disk, and then emplacing the surrogate UXO target on top of the grey surface (Figure 15). Data was then collected through the wave-dampening device in a variety of up- and down-ramp configurations. These configurations include {up 1 down 1}, {up 2 down 1}, {up 3 down 1}, {up 1 down 2}, {up 2 down 2}, {up 3 down 2}, {up 1 down 3}, {up 2 down 3}, and {up 3 down 3}. Preliminary contrast images were generated in the field to ensure a high quality data collect.

The surrogate UXO was then imaged with the MSI system, after correcting for saturation and look-angle artifacts of the experimental set-up. Finally, the surrogate UXO was placed directly upon the seafloor, sampled as above through the nine matrix combinations, and imaged through the wave-dampening device.

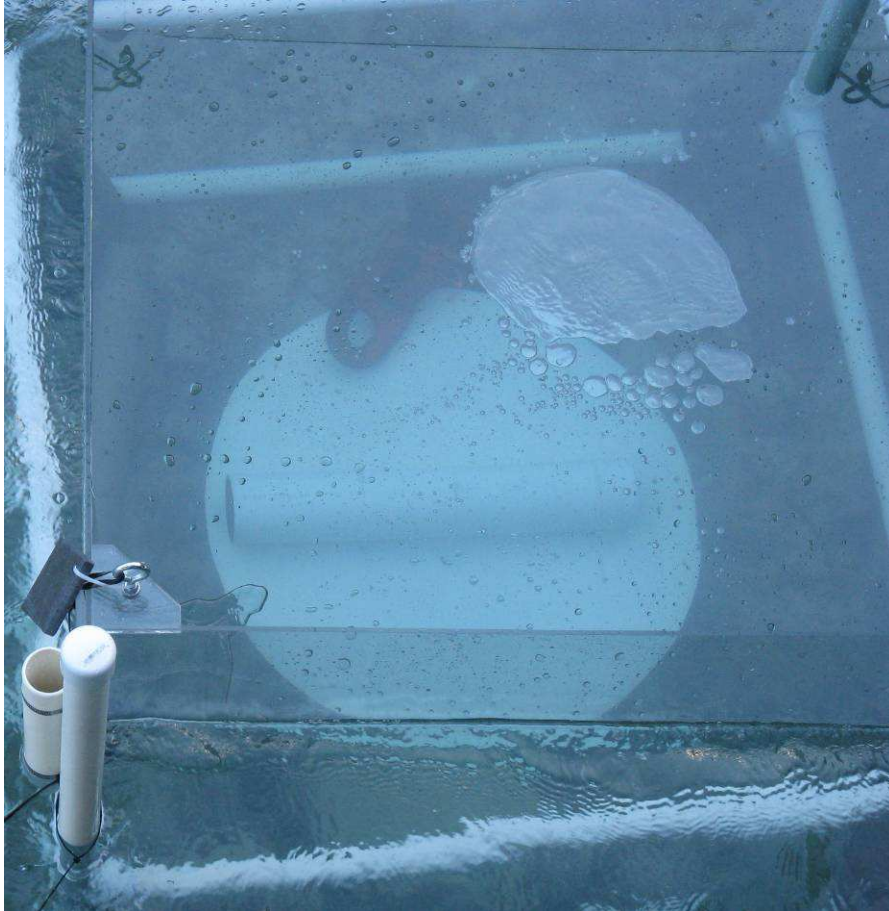


Figure 15. Deployed simulated shell and background plate within wave-dampening device.

4.4.2 Waikele Tunnel

The shearography system was tested for its utility in detecting UXO using a tunnel test facility at the Waikele Self Storage Facility on Oahu, HI. A plastic tub was used, reference BAE P/N 208301-001.

The target used was a shell 5 inches (127mm) in diameter and 21 inches in length. The shell had a 2 inch diameter hole through the length of the shell. The shell weighed 57 pounds. The shell was buried in a plastic tub with dimensions of 72 inch diameter and 24 inch depth. The tub was filled with 17 inches of construction-grade sand, which was kept moist for the duration of the test. The shell was buried at depths of 1.5 inch, 3 inch and 6 inch. Images were taken with the speaker placed at 0 degree, +45 degree and -45 degree as shown in Figure 16 and Figure 17.

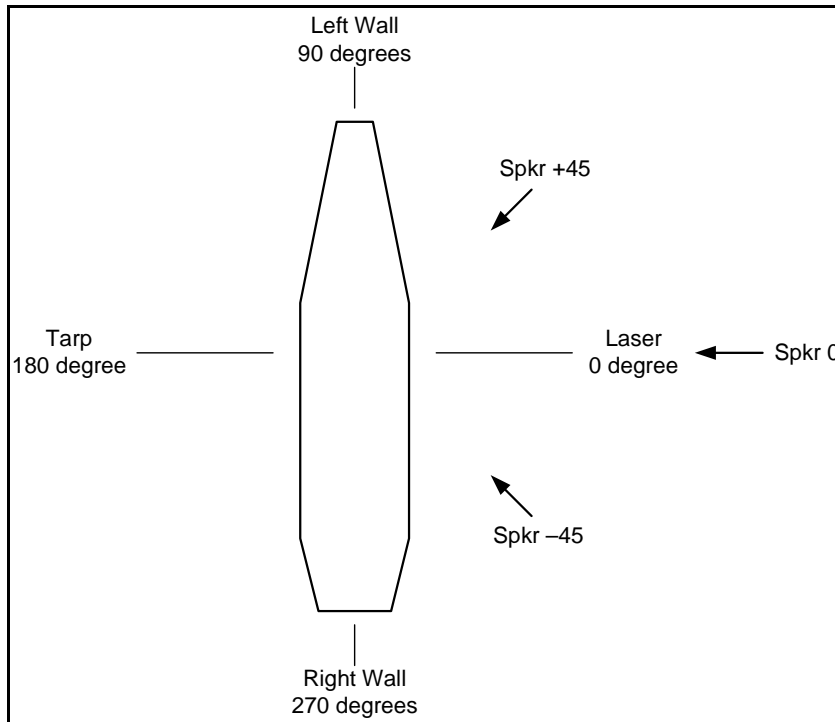


Figure 16. Target orientation 1 for shearography field test.

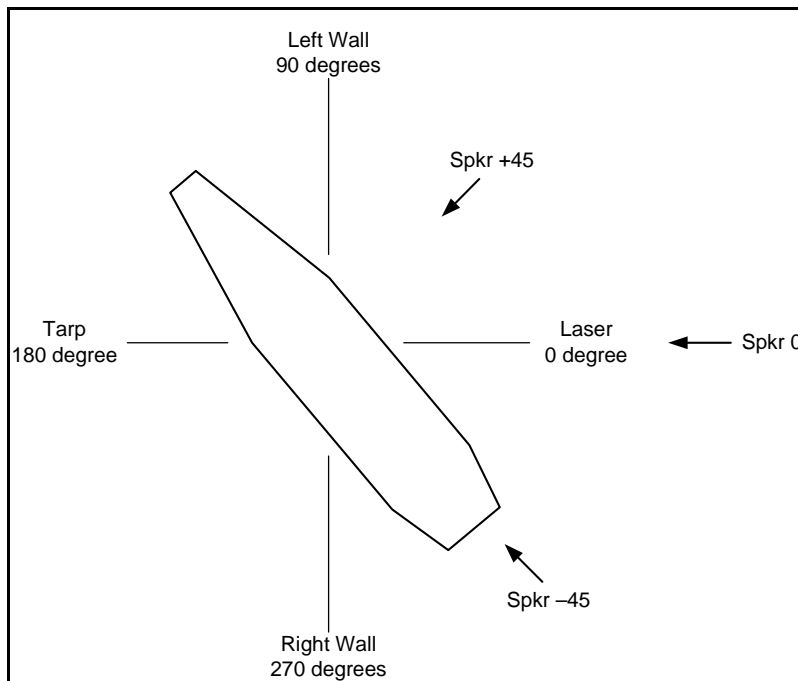


Figure 17. Target orientation 2 for shearography field test.

Targets were placed approximately in the center of the shearography camera's field-of-view. For each emplacement, an image with incandescent illumination was acquired to record the location of the target prior to burial. These emplacement images were used to draw outlines of the target

locations in the final processed shearogram images. The top surface of the sand was contoured to be flat, and parallel to the shearography platform to within $\pm 1^\circ$ along the direction of shear.

“Frequency Surveys” were performed to assess the frequency response of each target emplacement in the range of 40 to 500 Hz. At each frequency tested, a series of 12 shots (exposures) were acquired with successive phase offsets of 15° as described in Section 4.3.2. The standard protocol scanned frequencies from 40 to 500 Hz in 10 Hz increments.

The standard configurations for Frequency Survey experiments had:

- 75 mm, f/4 lens focused on the target surface,
- Insonification with 0.2V, 0.5V and 1V output signal sine-wave amplitude

The raw data acquired during each experiment consists of a series of images captured by the CCD camera. The images are processed in pairs to create the final shearograms.

Data recorded in a laboratory notebook for each experiment included:

- Time and date,
- Burial depth,
- Sand condition,
- Insonification frequency and SPL (power),
- Horizontal or vertical shear
- Other relevant observations and notes.

5.0 Results

5.1 Multi-Spectral Imagery

Due to the rapid bio-fouling of most underwater UXO, it was determined to use the edge detection approach on this imagery. Good (i.e., glint-free and in focus) imagery was obtained during the data collect that was representative of conditions that could be encountered by an airborne or surface-ship mounted sensor system (Figure 18). The contrast between the seabed and the targets varied considerably from band to band (see Band 1 vs. Band 2) as well as the general absorption and backscatter due to the water itself (Bands 3 and 6 vs Bands 4 and 5).

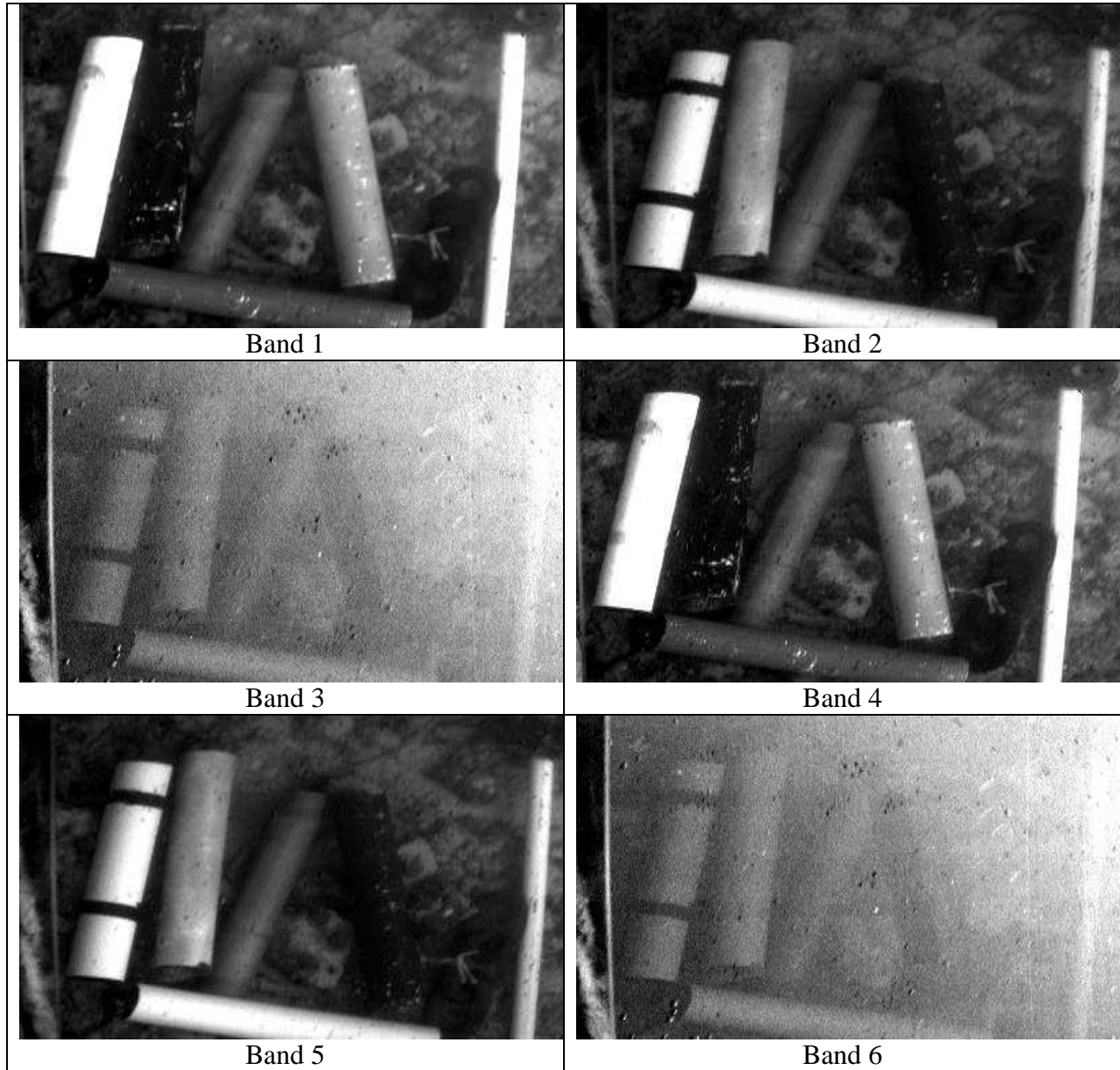


Figure 18. Grey scale images of each spectral band from the MSI sensor. Imagery was collected of all targets deployed during the Makai Pier test.

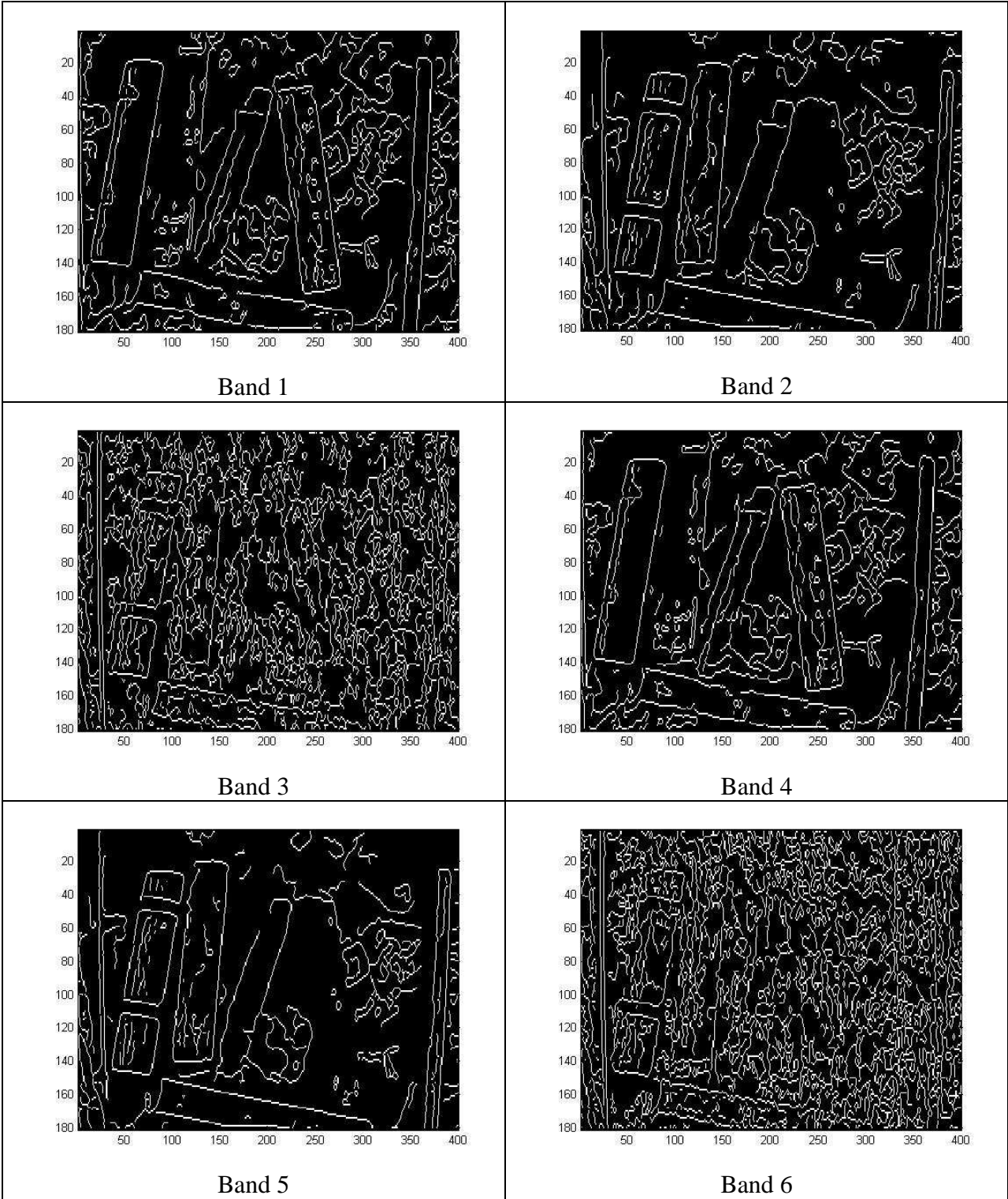


Figure 19. Output from the Canny edge detection algorithm applied to the imagery shown in Figure 18. Note the improved performance in the imagery in the water penetrating bands as opposed to the NIR.

Subsequently, the edge detection routine results (**Figure 19**) also varied significantly from band to band. Not surprisingly, those bands with the greatest penetration depth and backscatter produced the best output for denoting the outline of the surrogate targets. Those bands with significant backscatter or absorption resulted in significantly noisy edge-detection output.

Because it provides spectral information beyond what is available with standard camera technologies, MSI sensing provides a more robust way to detect un-natural or anomalous objects than does standard RGB imaging. At the same time, MSI provides very high spatial resolution, allowing edge and shape detection. The combination of morphology and spectrum has proven very useful in littoral mine-counter-measures projects.

5.2 REVEAL

Of the three imaging techniques investigated for this project, REVEAL showed the greatest technology maturity for through-water counter-UXO applications. The REVEAL imaging method offers the potential for determining the shape of ordnance on the bottom, detecting indicators of ordnance such as scour pits, and classifying bottom features. Because REVEAL is implemented with COTS range-gated cameras, large array sizes (on the order of a megapixel) are possible, providing detailed spatial information. In addition, the REVEAL technique operates the cameras in such a way that two range-gated snapshots can be used to extract the range to each pixel while automatically correcting for variations in illumination and reflectance. Thus, REVEAL LiDAR can work in situations, such as imaging through a distorting medium, in which purely passive shape-from-shading or stereoscopic methods are inapplicable. In addition, the REVEAL range resolution can use inexpensive long-pulse (nanoseconds) lasers to achieve resolution that would normally require picosecond laser with standard ranging lidar methods.

The application of REVEAL to shape-detection and clutter-discrimination in a relevant environment is illustrated in Figure 20 and Figure 21. These were created from 100 frames (3 seconds) of REVEAL imagery. They clearly show the 3D shapes of a 105-mm artillery shell, as well as man-made clutter consisting of anchor chain links and a section of PVC pipe, all laying on coral rubble. The vertical relief of the shell is accurate to ± 5 mm, despite the laser pulse width being 7 nanoseconds. For a normal lidar, this pulse width would yield a range resolution of 80 centimeters. Achieving 5-mm resolution with a conventional lidar would require sensing at 33-picosecond time resolution, requiring very expensive lasers and electronics, and current technology would still not achieve the high spatial resolution of REVEAL.

5.3 Shearography

This section presents the results of shearography detections from the frequency surveys. The most significant experimental conditions are listed in the figure captions along with a reference to the experiment's raw data identifier. The outline of the target emplacement is drawn in orange for reference and to aid in comparing fringe patterns at different depths.

The main purpose of the shearogram examination was to visually recognize revealing patterns that indicate buried objects. All shearograms from the data collect were visually inspected and images of interest were validated by other personnel.

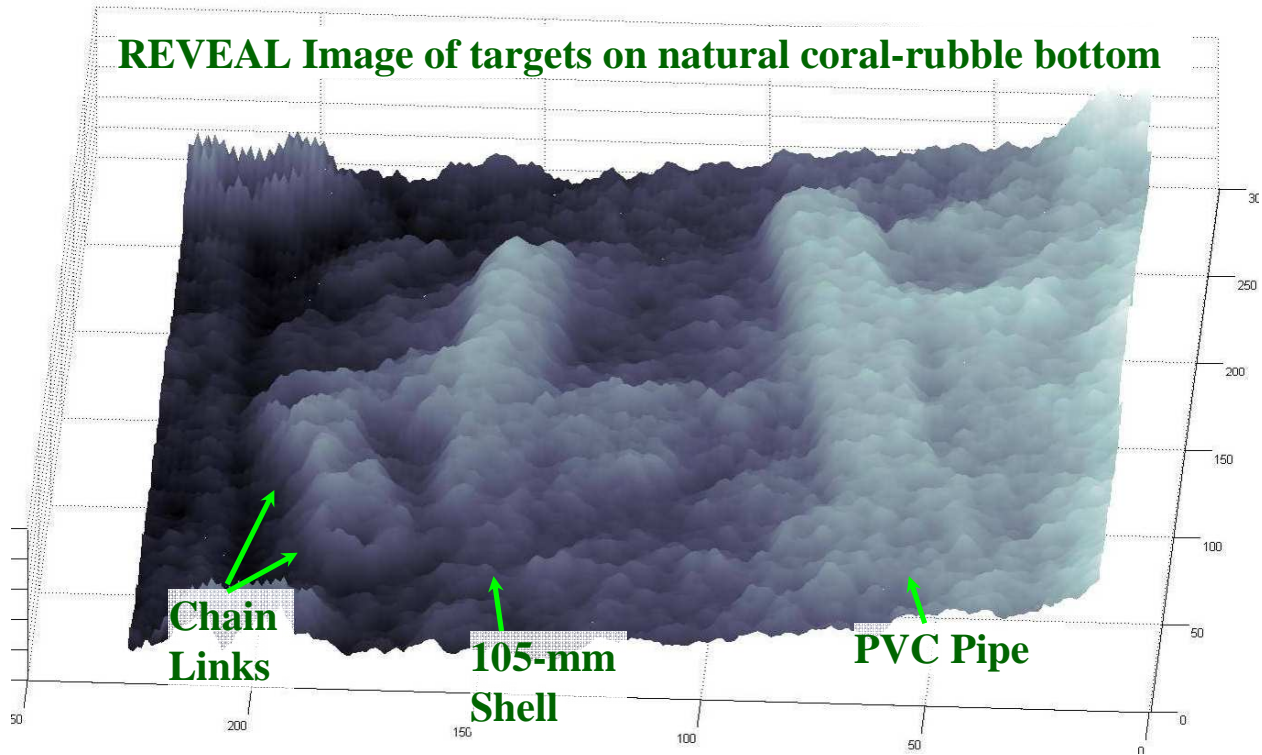


Figure 20. Top-down view of a final REVEAL elevation map. The UXO target was an orange shell on natural background imaged through the sea surface.

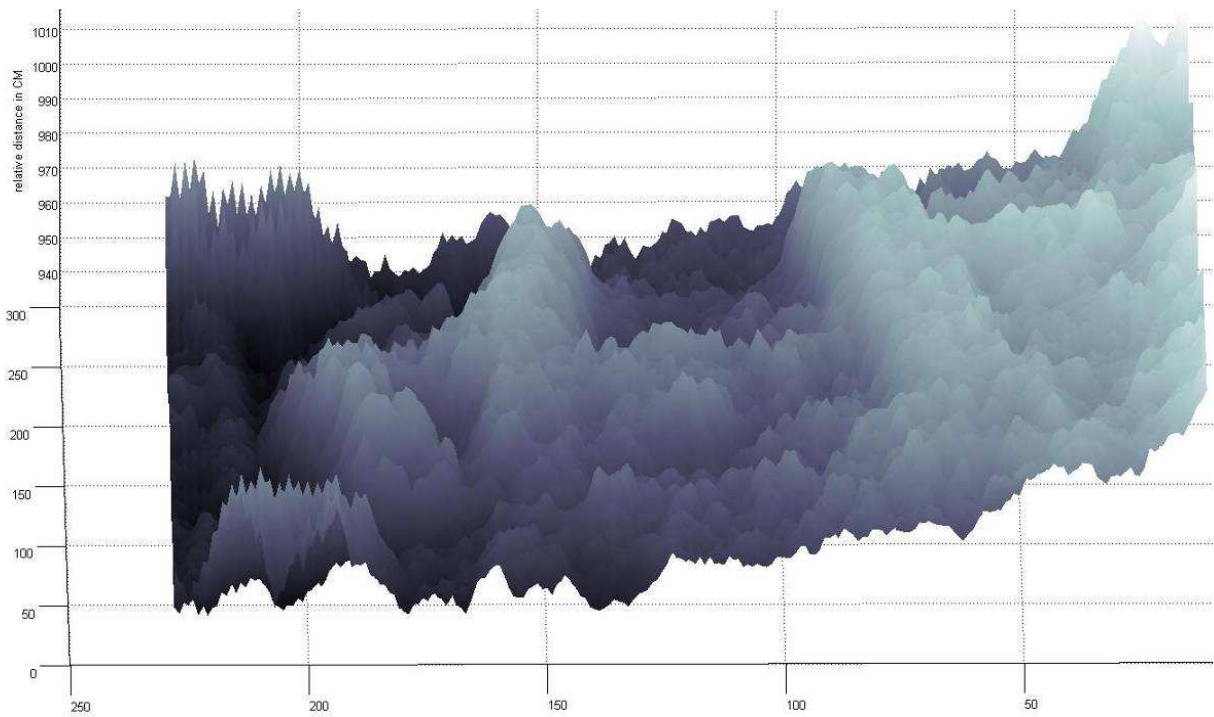


Figure 21. Profile (side) view of the ratio output. The scene is the same as in Figure 20. This view enables easier visualization of the actual height of the sample targets.

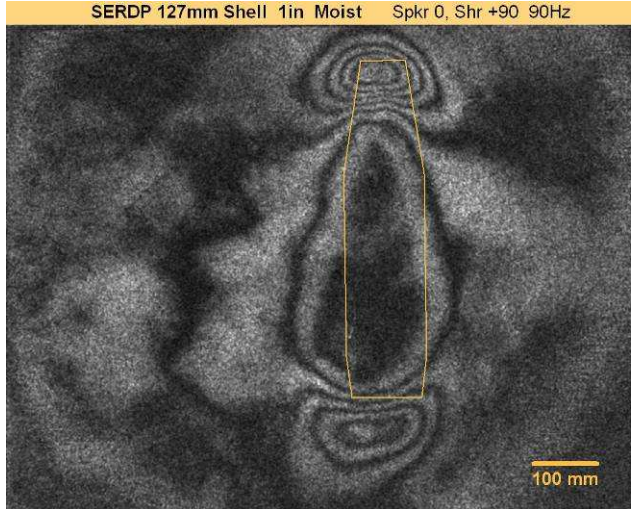


Figure 22. Shearogram of Shell, Depth = 1.5', Freq. = 90 Hz, Shear = Vert, Speaker = 0 deg. (Exper. 100323c_Run06_0304)

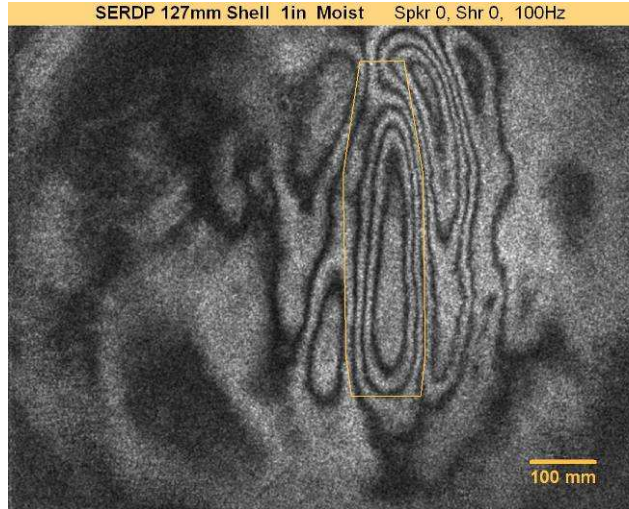


Figure 23. Shearogram of Shell, Depth = 1.5', Freq. = 100 Hz, Shear = Hor, Speaker = 0 deg. (Exper. 100323f_Run07_0506)

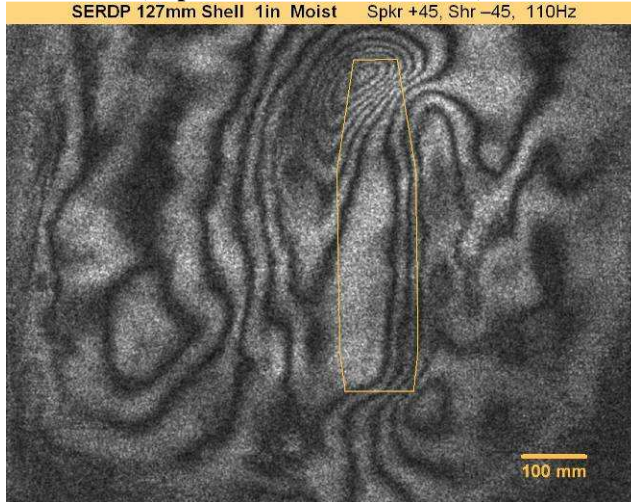


Figure 24. Shearogram of Shell, Depth = 1.5', Freq. = 110 Hz, Shear = -45, Speaker = +45 deg. (Exper. 100324b_Run08_1011)

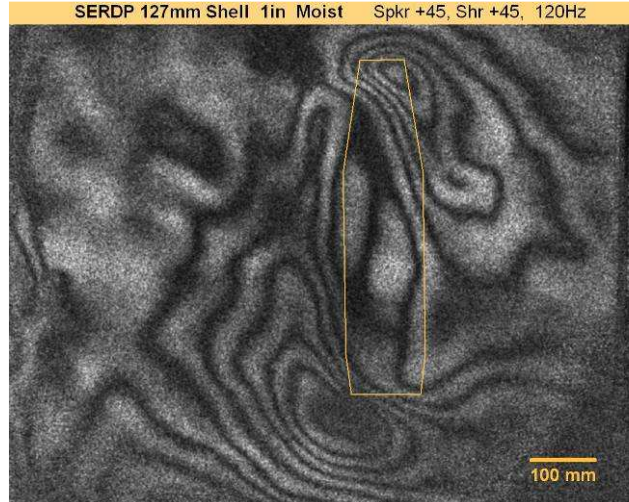


Figure 25. Shearogram of Shell, Depth = 1.5', Freq. = 120 Hz, Shear = +45, Speaker = +45. (Exper. 100324d_Run09_0405)

Both in the natural environment (the beach at Eglin Air Force Base) and in the Waikale tunnel tests, shallow-buried 155-mm shells showed distinct shearogram fringe patterns.

The primary challenge to using shearography for UXO detection is developing robust, automatic detection image-processing. Because Shearography is a new counter-ordnance technique, processing strategies have not yet been developed to optimize the processing and minimize human-in-the-loop effort. Identification and classification of targets in shearograms is a multi-step process, sketched in **Figure 26**: the fringe patterns must first be enhanced, then detected, and then the detected patterns must be characterized.

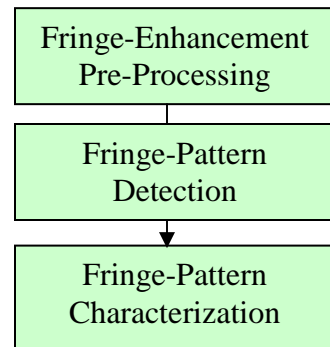


Figure 26. Shearogram analysis processing flow.

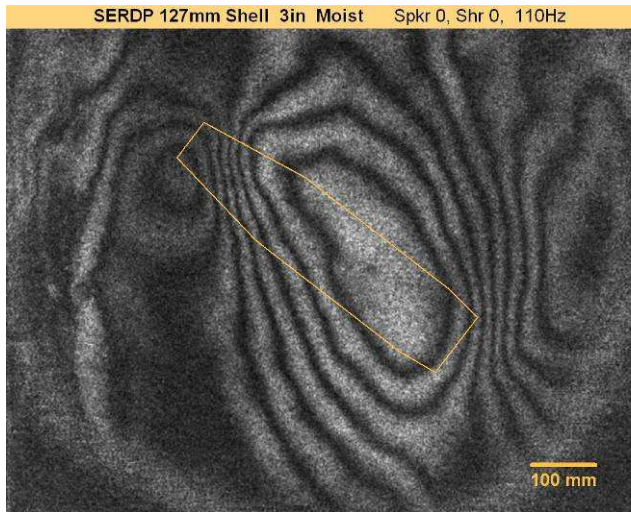


Figure 27. Shearogram of Shell, Depth = 3", Freq. = 110 Hz, Shear = Hor, Speaker = 0 deg. (Exper. 100324m_Run08_0203)

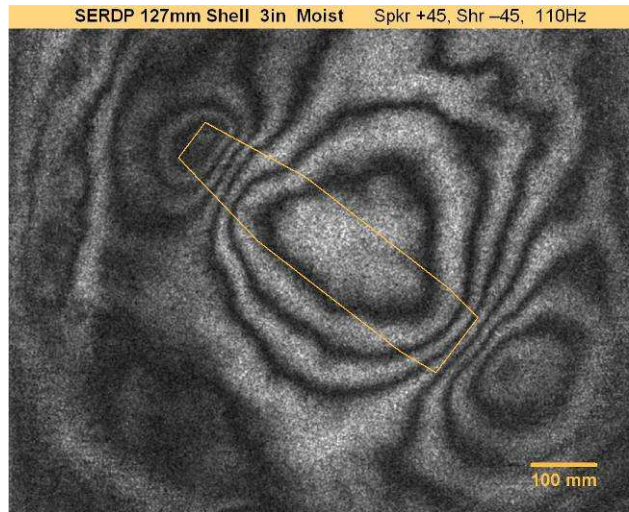


Figure 28. Shearogram of Shell, Depth = 3", Freq. = 110 Hz, Shear = -45, Speaker = +45 deg. (Exper. 100324r_Run08_0203)

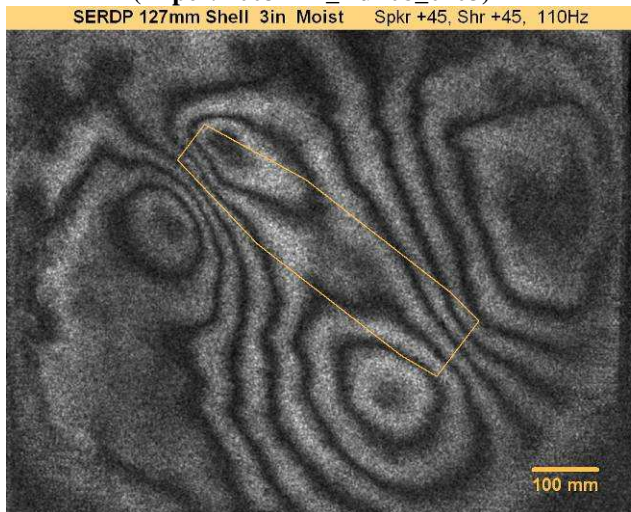


Figure 29. Shearogram of Shell, Depth = 3", Freq. = 110 Hz, Shear = +45, Speaker = +45 deg. (Exper. 100324t_Run08_0102)

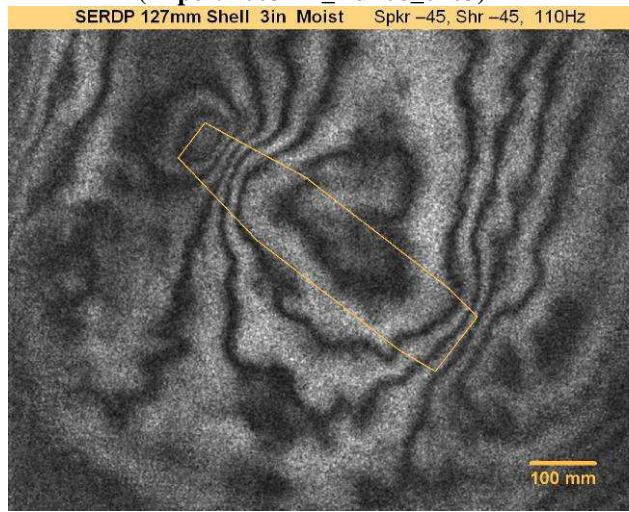


Figure 30. Shearogram of Shell, Depth = 3", Freq. = 110 Hz, Shear = -45, Speaker = -45 deg. (Exper. 100324x_Run08_0809)

The first step is enhancement of fringe patterns. The imagery itself is monochromatic, and potential targets (i.e., fringe pattern areas) do not differ from the background in either amplitude or variance, but only in the fine-scale distribution of a pixel values within the target region. Thus, identification of potential targets requires identifying local regions in which the *distribution* of values differs from the background areas.

One approach is to run a low-pass or band-pass filter on the shearogram, with an appropriately-sized convolution kernel. This will render background (fringeless) regions more uniform, while preserving the local intensity distributions within fringes. In addition to low-pass filtering, a normalization step is useful to remove local variations in illumination and background reflectance throughout the scene. This is important for equalizing the strength of fringe signals

so that fringes can be reliably detected throughout the image. Work remains to be done on automating the filtering and improving this normalization step, including how to reference a “standard” illumination for each portion of the image, what normalization math is most effective, and whether results are improved by normalizing before or after low-pass filtering.

Once filtering and normalization have been performed, it is necessary to identify the fringe patterns. At this stage of processing, fringe patterns will be areas that are darker and lighter than the mean image intensity. This provides several possible means for detecting fringes, including creation of local mean filters, local variances filters, and local SNR filters.

Once the fringe-containing regions are segmented, classification is possible. Since fringe morphology depends both on inherent target morphology, and on extrinsic factors such as soil properties and sensor characteristics, characterization of target morphology must rely on those features of the fringe pattern that are independent of non-target properties. Two such features would be size and shape (e.g., aspect ratio) of the fringe pattern. Here research involves refining and optimizing the pre-processing filtering steps outlined above, and then developing morphometric characterization algorithms to produce reliable measures of target shape and size.

The processing suite described above is outside the scope of MM-1630, but is being undertaken for ONR-sponsored counter-ordnance programs. Once the algorithms are available, their modification and extension to UXO detection will be straightforward.

Equipment Limitations Uncovered in Testing

Though we tested the shearography system for both wet and water-covered sand, we only obtained usable speckle fringes when there was *no* standing water on the surface. We traced this to the interplay of the limited coherence length of the laser and the index-matching effect of silica sand in water. By allowing the laser light to better-penetrate sand, a greater range of distances was sampled by the reflected laser beam. Since the coherence length of the laser used in the test was short, sampling multiple ranges simultaneously led to a scrambling of phase information in a way that was not retrievable. A secondary source of phase scrambling was the water-surface ripples, which evolved significantly over the time between laser pulses. The solution being implemented for the ONR program is to upgrade the system to use a long-coherence-length laser, and operate it at a repetition rate higher than the frequencies characteristic of surface-wave dynamics. Unfortunately, implementing these solutions and re-testing versus UXO is outside the scope and funding constraints of project MM1630.

6.0 Information Fusion and Automation

The greatest benefit to these results would be in combining the MSI spectra and edge detection output with imagery from REVEAL, shearography, or other detection modes. Both REVEAL and shearography give indications that there are man-made targets of interest in an area, while the edge detection has the potential to outline those targets and assign spectral characteristics. While any individual detection mode may have a limited Signal-to-Noise and Clutter ratio, the fusion can yield false-alarm rates much lower than any one sensing mode.

The next steps to turn the fused REVEAL and MSI technologies into a robust system for counter-ordnance applications include:

- Automated shape detection,
- Classification of shape (both 2D and 3D), spectrum, and range information into objects, backgrounds, and textures, and
- Automated identification of unnatural objects of interest.

While these are necessary tasks, the scope of data collection and algorithm refinement required are outside the scope of MM-1630, which was tasked to test existing technologies developed for mine-counter-measures programs. Once a robust counter-mine application suite and concept of operations is available, revisiting UXO detection and classification will likely be productive.

7.0 Conclusions and Future Direction

MSI and REVEAL Methodologies for Proud and Partially-Buried UXO

Together, MSI and REVEAL provide 4-dimensional (3 dimensions of space/shape and 1 dimension of spectrum). Collection of information sufficient for human-in-the-loop detection of proud ordnance on the sea bottom is feasible with MSI and REVEAL methodologies, but clutter rejection and automated processing still need to be demonstrated. The primary challenges will be the automation of the processing, which will require more data collections and algorithm development. In addition, the deployment strategies from various platforms (aircraft, surface vehicles, and unmanned underwater vehicles) need to be developed.

Because the optical systems are potentially very compact, and can work from above the surface, they are most suitable where sonar is unavailable or problematic, such as in extremely shallow or highly-stratified water. Since the constraints of mine countermeasures are likely to be very different from those of UXO remediation for these platforms, we recommend that separate UXO testing and development be undertaken for MSI and REVEAL either individually or in combination.

Shearography for Terrestrial Buried UXO

Shearography has been proven for land-based mine-countermeasures use, and the preliminary data for detecting buried artillery shells are promising, as shown in Figures 22-30. The key limitations are extending the thickness of soil penetrated by using improved acoustic projectors, and automating the detection and classification processing. Both these challenges are outside the scope of MM-1630, but are being addressed by ONR programs. Once the improved acoustic projectors and algorithms are available, we highly recommend that the improved technology also be tested versus non-mine UXO.

Shearography for Underwater Buried UXO

Shearography is aimed at solving the most-difficult counter-ordnance problem: buried ordnance underwater. Unfortunately, the available shearography systems had hardware limitations which precluded penetrating water-covered sand. The required technological fixes are outside the scope of MM-1630, but are being implemented under the ONR funded mine-countermeasures program. Once the new shearography system is available and has been tested versus mines (projected to be complete in 2011), we highly recommend that it also be tested versus non-mine UXO.

8.0 References

¹ http://www.eodcontractsltd.com/uxo_awareness.html

² Defense Cleanup and Environmental Programs: Authorization and Appropriations for FY2003
David M. Bearden, 2003

³ *Guidelines for Planning Unexploded Ordnance (UXO) Detection Surveys*, Simms, J.E., et al, 2004

⁴ www.uxoinfo.com/uxoinfo/downloads/UnderwaterUXO_EnvEffects.pdf

⁵ <http://www.naevageophysics.com/newsart2.html>

⁶ *Seismic Imaging of UXO-Contaminated Underwater Sites*, Gritto, et al UC Berkeley, 2001

⁷ *Mobile Underwater Debris Survey System (MUDSS) Summary*" McCormick, J.F. et al Coastal Systems Station, Panama City, FL, 1999

⁸ Jerlov, N.G., 1976, *Applied Optics*. (Amsterdam: Elsevier Scientific Publishing Company).

⁹ W. Steinchen and L. Yang, *Digital Shearography, Theory and Application of Digital Speckle Pattern Interferometers*, SPIE Press, 2003.